The Mesoproterozoic Stac Fada Member, NW Scotland: An impact origin confirmed but refined

Abbreviated title: Origin of the Stac Fada Member

G. R. Osinski[1,2]*, L. Ferrière[3], P. J. A. Hill[1,2,4], A. R. Prave[5], L. J. Preston[6], A. Singleton[1,2] & A. E. Pickersgill[7]

[1]Department of Earth Sciences, University of Western Ontario, London, Ontario, N6A 5B7, Canada.

[2]Institute for Earth and Space Exploration, University of Western Ontario, London, Ontario, N6A 5B7, Canada.

[3]Natural History Museum, Burgring 7, A-1010 Vienna, Austria.

[4]Department of Earth and Atmospheric Sciences, University of Alberta, Edmonton, Alberta T6G 2E3, Canada

[5]School of Earth and Environmental Sciences, University of St Andrews, St Andrews, Fife, KY16 9AL, Scotland

[6]Department of Earth Sciences, The Natural History Museum, Cromwell Road, London, SW7 5BD, United Kingdom

[7]School of Geographical and Earth Sciences, University of Glasgow, Glasgow, G12 8QQ, United Kingdom

*Correspondence: gosinski@uwo.ca

Abstract: The origin of the Stac Fada Member has been debated for decades with several early hypotheses being proposed, but all invoking some connection to volcanic activity. In 2008, the discovery of shocked quartz led to the hypothesis that the Stac Fada Member represents part the continuous ejecta blanket of a meteorite impact crater, the location of which was, and still remains, unknown. In this contribution, we confirm the presence of shock-metamorphosed and -melted material in the Stac Fada Member; however, we also show that the properties of the Stac Fada Member are unlike any other confirmed and well documented proximal impact ejecta deposits on Earth. Instead, the properties of the Stac Fada Member are most similar to the Onaping Formation of the Sudbury impact structure (Canada) and impact melt-bearing breccias from the Chicxulub impact structure (Mexico). We thus propose that, like the Sudbury and Chicxulub deposits, melt-fuel-coolant interactions – akin to what occurs during phreatomagmatic volcanic eruptions – played a fundamental role in the origin of the Stac Fada Member. We conclude that these rocks are not primary impact ejecta but instead were deposited beyond the extent of the continuous ejecta blanket as high-energy ground-hugging sediment gravity flows.

Introduction

Over the past several decades, there has been a growing awareness of the importance of impact cratering as an important and, indeed, fundamental planetary geological process (Melosh 1989; Osinski & Pierazzo 2012; Grieve 2017). The ever increasing exploration of Solar System bodies by robotic spacecraft has returned a wealth of data on meteorite impact craters; however, the impact cratering record on Earth remains critical and necessary for ground-truthing planetary observations due to the ability to conduct fieldwork, detailed geophysical surveys, and to obtain samples with known context. The number of confirmed meteorite impact craters on Earth stands at approximately 200 (Osinski & Grieve 2019; see also www.impactearth.com for an up-to-date inventory). It is notable that there remains no confirmed impact crater in the British Isles, although the existence of both distal and proximal impact ejecta layers have been proposed from SW England (Walkden *et al.* 2002) and the Scottish Highlands (Amor *et al.* 2008; Drake *et al.* 2017). Of these, the Stac Fada Member, part of the Torridonian Supergroup, has received most attention to date and is the focus of this study.

The ~1.2–1.0 Ga Torridonian Supergroup of NW Scotland comprises a succession of mostly reddish-brown sandstones as much as 8 km thick that rest unconformably on Neoarchaean rocks of the Lewisian gneiss complex (Stewart 2002). These distinctive rocks dominate the landscape of this region, forming prominent mountains. It is divided, from oldest to youngest, into the Stoer, Sleat and Torridon Groups. The Stac Fada Member is part of the Stoer Group (Fig. 1) and was initially thought to be volcanic in origin; ideas varied from an ash flow deposit related to hydroclastic eruptions (Lawson 1973), a hot mudflow generated by magma intruded into wet sediment (Sanders & Johnston 1989), to a volcanic debris flow (Stewart 2002; Young 2002). In 2008, Amor *et al.* (2008) proposed that the Stac

Fada Member was an impactite (i.e., a rock affected by hypervelocity impact resulting from the collision of planetary bodies; Stöffler & Grieve 2007) called "suevite", forming the proximal ejecta blanket of a meteorite impact structure. These conclusions were based on the presence of shocked quartz grains (and biotite with kink bands, which are not, however, diagnostic of shock; French & Koeberl, 2010), chromium isotopes and elevated platinum group metal and siderophile element abundances. More recently, these authors referred to the Stac Fada Member as an impact melt rock (Amor *et al.* 2019). The discovery of reidite ($ZrSiO_4$) provided further evidence of an impact origin (Reddy *et al.* 2015). The location of the source crater remains unresolved: one suggestion is The Minch (Fig. 1), northwest of the outcrop belt (Amor *et al.* 2019), and the other is the Lairg Gravity Low (Fig. 1) (Simms 2015; Simms & Ernstson 2019), which, if correct, has significant implications for the deep crustal structure of northern Scotland (Butler & Alsop 2019; Simms 2019; Simms & Ernstson 2019).

The motivation for our study was three-fold. Firstly, continuous impact ejecta blankets are rare on Earth due to their rapid erosion hence the Stac Fada Member could provide insight into ejecta emplacement on terrestrial planets (Branney & Brown 2011; Osinski *et al.* 2011). Secondly, very low amounts of shocked material combined with high glass abundance (Amor *et al.* 2008) and high degree of sorting are at odds with observations of other known impact ejecta deposits (Osinski *et al.* 2011, 2012) and this deserves explanation. Thirdly, the mechanism of emplacement of the Stac Fada Member remains a subject of debate. Here we provide additional documentation of shock features, further reinforcing the impact origin of material contained within the Stac Fada rocks. We offer, though, an alternative hypothesis for their genesis, one based on recent understanding of impactites associated with the Sudbury (Canada) and Chixulub (Mexico) impact structures, both of whose origins are attributed to molten-fuel-coolant interaction analogous to what occurs during phreatomagmatic volcanic eruptions (Grieve *et al.* 2010; Osinski *et al.* 2020).

Geological setting of the Stac Fada Member

The Mesoproterozoic Stoer Group defines a patchily preserved outcrop belt extending for ca. 50 km along the NW coastal area of Scotland (Fig. 1). It is the oldest non-metamorphosed sedimentary rock unit in Britain, consisting predominantly of fluvial sandstone as much as 2.5 km thick and divided into the Clachtoll, Bay of Stoer, and Meall Dearg formations (Stewart 2002). The Bay of Stoer Formation is further divided into the Stac Fada and Poll a'Mhuilt members. The lithostratigraphy follows that of Stewart (2002) as amended by Simms (2015). Potassium feldspar veins of presumed hydrothermal origin in the Stac Fada Member yield an $^{40}Ar/^{39}Ar$ age of 1177 ± 5 Ma (Parnell *et al.* 2011).

The Stac Fada Member contains accretionary lapilli and abundant chloritized shards interpreted as former glass fragments. The latter two features are unique to the Stac Fada Member within the Torridonian succession and are key components in assessing its origin. Also important to note is that the overlying Poll a'Mhuilt Member was originally thought to be lacustrine (Stewart 2002), potentially formed due to drainage disruption by the effects of the impact (Amor *et al.* 2008; Simms 2015), but recently has been shown, in part, to be estuarine in origin (Stüeken *et al.* 2017).

Samples and methods

Fieldwork was carried out to investigate the Stac Fada Member on multiple occasions from 2008 to 2016. This unit was studied and sampled at 5 localities, with samples being collected with a chisel and rock hammer (Fig. 1). Optical microscopy was performed on polished thin sections from 46 samples using an optical microscope at up to 200x

magnification combined with a four-axis universal-stage (U-stage) (Emmons 1943). The entire area of each thin section was examined and all quartz grain properties recorded, i.e. unshocked, shocked with planar fractures (PF), shocked with planar deformation features (PDF), number of sets of PFs and PDFs, presence of PDF decoration, and the overall appearance. The exact position of each shocked quartz grain was noted on a thin section map and crystallographic orientations of PF and PDF sets in shocked quartz grains were measured using the U-stage microscope, following the methods described in the literature (e.g. Engelhardt & Bertsch 1969; Stöffler & Langenhorst 1994; Ferrière *et al.* 2009a). Indexing of PDF sets was done with the Automated Numerical Index Executor (ANIE) program (using the average value of measurements and a 5° error; Huber *et al.* 2011).

Quantitative analyses and investigation of micro-textures were carried out using both back-scattered electron (BSE) imagery and wavelength dispersive X-ray (WDS) techniques on a JEOL JXA-8900 L electron microprobe. Electron microprobe data were reduced using ZAF procedures incorporated into the operating system.

Semi-automatic digital image analysis was conducted to quantify the geometry of clasts in hand samples to compare them to previously collected and published data on hand samples of other glass-bearing breccias from confirmed and well-studied impact ejecta deposits at the Ries (Germany) and Mistastin Lake (Canada) impact structures, together with similar glass-bearing breccias from the Sudbury (Canada; i.e., the Onaping Formation) and Chicxulub (Mexico) impact structures (Osinski *et al.* 2016, 2020; Hill *et al.* 2020). Following the methods of Chanou *et al.* (2014), particles of interest (POI) (i.e., vitric particles) were segmented and measured using the National Instituted of Health's digital imaging freeware, ImageJ. RGB images were contrasted so that vitric particles and associated features could be binned. If the contrast between the POI and the background was high enough, POIs were segmented by splitting the three colour channels and thresholding the resulting 8-bit grayscale

image. If the original image contrast was not high enough, background subtraction allowed for isolation of clasts prior to splitting channels and segmenting the 8-bit grayscale image. Following segmentation of the POIs, the 8-bit grayscale images were manually corrected for any lighting, deformation, or image artefacts that could have been incorrectly segmented. Particle analysis was then conducted allowing for determination of area, perimeter, area fraction, shape descriptors and fractal dimension.

Field relations and petrography

The main characteristics of the Stac Fada Member are summarised in Table 1. We use the descriptive term "melt-bearing breccia" for the Stac Fada Member to reflect the fact that it contains material that was formerly molten and that overall, it is a rock that contains angular clasts >2 mm in diameter surrounded by a finer grained matrix; a caveat is that there are small areas where, in outcrop and hand sample, the Stac Fada Member could be classified as a sandstone. We also use the term "vitric" to describe the green clasts that were originally glass but are now completely devitrified and altered, although original morphologies are well preserved.

Bay of Stoer. This is the type locality of the Stac Fada Member. There, melt-bearing breccia occurs in four main units (Young 2002), with the lower units resting sharply on and interbedded with sandstone of the Bay of Stoer Formation and containing several large (up to ~14 m long), tabular rafts of Bay-of-Stoer sandstone (Fig. 2). The basal unit (SF1 of Young (2002)) is up to 3.2 m thick, sits sharply on underlying sandstone, and consists of a thin basal melt-free pebbly sandstone that grades upward over ~10 cm into typical vitric-bearing melt breccia. At low tide, it can be seen that the western contact of this basal unit is a fault, leading to the interpretation by some workers (e.g., Young 2002)) that this is not a separate layer but

rather a faulted offset of the main uppermost layer described below. We could not confirm this and the lack of accretionary lapilli and fluid escape pipes that are seen in SF4 (see below) suggests that this may be a separate unit offset by an unknown amount from the other units. The next two units are wedged-shaped: the first (SF2) is ~1.5 m thick and the second (SF3) is a few cm to dm-thick; both taper and pinch-out towards the northern end of the outcrop (a distance of 10–15 m). Young (2002) considered these as discrete units but our observations suggest they are apophyses extending from the overlying unit. In other words, the three main Stac Fada Member units are continuous with each other (cf., Amor *et al.* 2008, 2019; Stewart 2002).

The uppermost melt-bearing breccia unit (SF4 of Young, 2002) averages ~12 m in thickness (Figs. 2a,b). This unit is typified by vitric clasts, <0.1 to ~1 cm across (Fig. 2c) and contains rounded to sub-rounded clasts of gneiss up to ~50 cm across (Fig. 2d). It has an erosional base and contains large (up to ~14 m long) sandstone clasts near the base (Figs. 2a,b). These sandstone clasts are typically planar with shape controlled by the bedding; the sandstones appear to all be locally derived. Overall, this main Stac Fada Member unit appears massive, although crude indistinct bedding on the mm- to cm-scale is discernable towards the top and base; this bedding is much easier to see on polished hand specimens than in the field. Sub-vertical, honeycomb-like structures (fluid escape pipes of Amor *et al.* 2008 and Parnell *et al.* 2011) filled with authigenic feldspar are present throughout this unit. Rounded accretionary lapilli (~2 – 6 mm diameter; average ~2 mm) are dispersed through the uppermost 3 m but are concentrated in discontinuous lenses near the top of the unit. The Stac Fada Member is overlain sharply by several metres of channelled sandstone, identical to the underlying Bay of Stoer Group (see Fig. 1 of Stüeken *et al.* 2017). The sandstones contain reworked clasts of impact melt-bearing breccia and accretionary lapilli and the contact with the Stac Fada melt-bearing breccia locally shows deep erosive scours into the Stac Fada

194 breccia (Fig. 2e). The sandstones pass upward over a few metres into grey and red mudstones
195 of the Poll a'Mhuilt Member.
196 In hand specimen and thin section, the vitric particles are dispersed in a clay to sand-
197 sized matrix and all are altered (Figs. 2c, 3a,b, 4). Image analysis of four samples delineated
198 6,124 vitric particles with mean size of 0.2–0.4 mm with textures from shard-like and vesicle-
199 free to vesicular with flow textures (Figs. 4a–c). Vesicles are generally elongate and many are
200 infilled with secondary minerals (Fig. 4c). It is notable that schlieren and quench crystallites –
201 typical for impact glasses (Stöffler 1984) – are lacking in the samples we have studied (Table
202 1). Some vitric clasts contain undigested quartz and, more rarely, feldspar grains.
203 ***Rubh' a' Choin, Enard Bay.*** The Stac Fada Member is thickest (~20 m) at this
204 locality and comprises a single unit. The bulk of the member at this location is the
205 characteristic glass-bearing breccia similar to the main upper unit at the Bay of Stoer. The
206 major difference is towards the top where the upper 2–3 m is dominated by accretionary
207 lapilli (Figs. 2e, 3c, 4d); fluid escape pipes are also notably absent. Layering on the mm to
208 dm-scale is occasionally present (cf., Gracie & Stewart 1967). It occurs above a variably thick
209 interval of interbedded sandstone and sedimentary breccia of the Clachtoll Formation (Fig. 2f)
210 (e.g., Stewart 2002). Amor *et al.* (2019) interpreted these underlying rocks to be a
211 consequence of ballistic fragmentation along the outer layer of a collapsing ejecta blanket.
212 However, careful inspection shows that these rocks are no different to the Clachtoll Formation
213 elsewhere hence are most parsimoniously and objectively interpreted as material derived by
214 normal erosional processes that formed the irregular palaeotopography observed everywhere
215 along the contact of the Stoer Group and Lewisian gneiss complex.
216 ***Outcrops elsewhere.*** The remaining outcrop localities of the Stac Fada Member south
217 of Enard Bay are mostly thinner (<10 m thick) and their field and petrographic characteristics
218 have been described in detail by Simms (2015) and, although differences exist between

219 localities, the general character of the Stac Fada makes it recognisable from location to
220 location. A notable exception is the ~7 m thick outcrop at Stattic Point in which accretionary
221 lapilli are absent but vitric clasts are at the highest concentrations and exhibit the largest sizes,
222 as much as ~15 cm across (cf., Amor *et al.* 2008; 2019). This outcrop also displays distinctive
223 curved fractures that penetrate ~1 m into the outcrop and that do not continue into the
224 overlying sandstone of the Poll a'Mhuilt Member. Simms (2015) interprets these features as
225 ogive fractures or synsedimentary shear surfaces that develop on or near the surface of
226 mudflows and other slowly moving viscous materials.
227 ***Textural image analysis.*** The Stac Fada Member is often described as being poorly
228 sorted. However, that is only relative to the encasing sandstones. More importantly for this
229 study is how the Stac Fada Member compares to glass-bearing breccias from other well-
230 studied impact structures where the stratigraphic context and setting with respect to the host
231 crater is known. Thus, using the semi-automated image analysis methodology of Chanou *et*
232 *al.* (2014), we quantified the degree of sorting of the Stac Fada breccias with respect to a
233 calibrated sorting scale and compared this to data from other glass-bearing impact breccias.
234 Specifically, we compared the Stac Fada Member to the two best-preserved and exposed
235 examples of glass-bearing proximal ejecta deposits on Earth (the Ries (Engelhardt 1990) and
236 Mistastin (Mader & Osinski 2018) impact structures), together with glass-bearing breccias
237 from the Onaping Formation from the Sudbury impact structure (Grieve *et al.* 2010) and the
238 Chicxulub impact structure (Osinski *et al.* 2020) (Figs. 5, 6). These results clearly show that
239 the Stac Fada Member is markedly different to the Ries and Mistastin ejecta deposits, in that it
240 is moderately to very well sorted, but displays similar properties to the Sudbury and
241 Chicxulub glass-bearing breccias.
242
243 **Shock metamorphic indicators**

Due to the high pressures generated during the impact cratering process (up to and exceeding 100 GPa), rocks and minerals can undergo a series of transformations and produce a range of characteristic and diagnostic shock metamorphic effects (see French & Koeberl 2010, for a review). The presence of planar deformation features (PDFs) in quartz provides unequivocal diagnostic evidence for meteorite impact events (French & Koeberl 2010) and, as such, was a high priority during our investigations. It is notable that we found no evidence of shock metamorphism in 30 clasts of shocked gneiss that we investigated; rather, shock effects are restricted to mineral clasts as described below. The absence of shock-metamorphic effects in lithic clasts is in stark contrast to impact melt-bearing ejecta from other impact craters, such as the Mistastin and Ries impact structures, but is in keeping with observations of the Onaping Formation from the Sudbury impact structure and the melt-bearing breccias from the Chicxulub impact structure (Table 1).

In terms of the shock mineral grains, compared to other impact craters, the Stac Fada Member has a minimal amount of shocked quartz (Table 1). What shocked quartz is present, though, is varied (Table 2) and includes undulose extinction, PFs and/or PDFs, mosaicism and a few grains with patches of micrometre-scale fluid inclusions and a greyish-brown appearance (Fig. 7a), described by some workers as “toasted” (Whitehead *et al.* 2002; Ferrière *et al.* 2009b). The maximum number of shocked quartz grains with PFs and/or PDFs in any one thin section was eight. Occasionally, PFs and PDFs occur together in the same quartz grain. Typically, quartz grains contain one or two sets of PDFs (Figs. 7b–d), and more rarely three (Fig. 7e) or four sets were observed under the U-stage (Table 2). The PDFs are frequently decorated with numerous tiny fluid inclusions, and, thus, are more easily detected as compared to the less visible, non-decorated PDFs. It can be explained in part that additional PDF sets, not visible under the optical microscope, were detected (and measured) under the

U-stage microscope (Fig. 8). Similar observations were reported in the detailed study of shocked quartz from the Bosumtwi crater (Ghana) by Ferrière *et al.* (2008).

Because specific crystallographic orientations of PDFs in quartz grains are formed at different shock pressures (see e.g., Hörz 1968; Müller & Défourneaux 1968; Huffman & Reimold 1996), crystallographic orientations of PDF sets can be used to constrain the peak shock pressure that these grains have experienced. The crystallographic orientations of 90 PF and PDF sets in 59 shocked quartz grains from 18 thin sections were measured with the U-stage. Data in absolute frequency % are reported in Table 3 and absolute frequency % of indexed PDF sets versus angle between the c-axis and poles to PDF planes is shown in Figure 8. A large proportion, 63 absolute frequency percent, of all the poles to the PDF planes measured are oriented parallel to the $\omega\{10\bar{1}3\}$ orientation. In addition, about 14 absolute frequency percent of the measured PDF sets are parallel to the $\{10\bar{1}4\}$ orientation and also to the $\pi\{10\bar{1}2\}$ orientation, whereas, planes parallel to the c(0001), $\{2\bar{1}\bar{3}1\}$, and $\{22\bar{4}1\}$ orientations are also present (Table 3; Fig. 8), but in somewhat lower proportions. It should be noted that because it is impossible to uniquely distinguish between $\{10\bar{1}4\}$ and $\{10\bar{1}3\}$ orientations using the U-stage when the angle between c-axis and poles to PDF is about 18–23°, all measured planes that fall into the overlap zone between $\{10\bar{1}4\}$ and $\{10\bar{1}3\}$ orientations are considered as $\{10\bar{1}3\}$ orientations for the purpose of our U-stage analysis, as recommended by Ferrière *et al.* (2009a).

Only two quartz grains with PDFs were found in vitric clasts from two separate samples (Tables 1, 2), one had two PDF sets with $\{10\bar{1}3\}$ orientations and the other had one highly decorated PDF set with $\{10\bar{1}4\}$ orientation. Two shocked quartz grains were found in lapilli in one sample with one PF set orientated at $\{10\bar{1}0\}$ and another at $\{10\bar{1}3\}$. A few feldspar grains were observed that were highly fractured, but these, too, did not display shock-related features. Kink bands were observed in muscovite and in chlorite grains. However, kink bands

294 in micas are common in metamorphosed and deformed rocks (e.g., Lewisian gneiss) and
295 cannot be used as criteria for an impact origin.
296
297 **Discussion**
298
299 ***Confirming the presence of shocked material in the Stac Fada Member***
300
301 During meteorite impact events, pressures and temperatures are sufficient to vaporize,
302 melt, and/or metamorphose a substantial volume of the target sequence (e.g., French &
303 Koeberl 2010; Osinski *et al.* 2018). A variety of characteristic shock metamorphic indicators
304 are produced, such as shatter cones, PDFs, and diaplectic glasses (French & Koeberl 2010;
305 Ferrière & Osinski 2012). Amor *et al.* (2008) identified PDFs in 25 quartz grains from 9 thin
306 sections. Our observations from 46 thin sections confirm the presence of PDFs in quartz. We
307 documented 78 PDF sets in 48 quartz grains (Table 2), which is a notably lower PDF-plane-
308 to-grain ratio, 1.63, than the 2.36 reported by Amor *et al.* (2008). This difference of results is
309 not surprising, as Amor *et al.* (2008) measured only 25 quartz grains in nine thin sections as
310 compared to the 78 PDF sets in 48 quartz grains in this study. In addition, the U-stage results
311 of Amor *et al.* (2008) left with 31% of PDF sets unindexed, raising questions about how
312 representative their results are (Ferrière *et al.* 2009a).
313 Based on our U-stage results, PDF orientations parallel to $\{10\bar{1}3\}$, like those measured
314 in our work, require shock pressures between 12–20 GPa (Stöffler & Langenhorst 1994), with
315 some workers suggesting a minimum required of 16 GPa (Hörz 1968). The presence of vitric
316 clasts suggests that pressures could have been greater than ~50 GPa given that the impact was
317 in hard and/or crystalline rocks (Stöffler 1972, 1984; Osinski *et al.* 2018). Thus, our results
318 corroborate the findings of Amor *et al.* (2008) and Reddy *et al.* (2015) and further confirm

319 that the Stac Fada Member contains material derived from an impact event. However, the
320 amount of shocked material in the Stac Fada Member is extremely low compared to other
321 impact ejecta deposits (Table 1) (see also the recent detrital zircon and apatite study by Kenny
322 *et al.* (2019)), which we discuss further below.
323
324 ***6.2. The Stac Fada Member: a continuous impact ejecta deposit?***
325
326 Impact ejecta deposits can be defined as target materials transported beyond the rim of
327 the transient cavity (Osinski *et al.* 2011). It is widely accepted that the initial emplacement of
328 a continuous ejecta blanket around impact craters is via ballistic sedimentation (Oberbeck
329 1975) in which ejected material follows a nearly parabolic flight path before striking the
330 surface at some percentage of the velocity that it possessed when ejected. Upon landing, this
331 primary ejecta continues to flow across the surface, generating considerable erosion and
332 incorporation of local material (i.e., "secondary ejecta"), thereby modifying the region
333 surrounding the host crater (Oberbeck 1975; Hörz 1982). Acknowledging that the target rock
334 influences the final characteristics and radial extent of ejecta blankets (e.g., Oberbeck 1975;
335 Hörz 1982; Barlow 2005; Osinski *et al.* 2011), the preserved remnants of well-studied
336 continuous ejecta blankets (e.g., the Bunte Breccia at the Ries impact structure and Meteor
337 Crater ejecta deposits) exhibit three common features: (i) abundant material shocked to low
338 pressures, (ii) a dearth of high shocked and shock-melted material (i.e. vitric clasts), and (iii)
339 very poor sorting with blocks reaching 100s of m to km in size (Shoemaker 1963; Hörz 1982;
340 Hörz *et al.* 1983). While the low amount of shocked material is a common trait, it is clear that
341 the Stac Fada Member bears little resemblance to the continuous ejecta blankets of simple
342 (e.g., Meteor Crater) or complex (e.g., Ries) impact structures. Most critical is the overall well
343 sorted nature and the preponderance of vitric clasts in the Stac Fada Member. Thus, ballistic

emplacement can be ruled out for its emplacement (cf., Branney & Brown, 2011). Regarding the idea that isolated blocks of gneiss in sandstones immediately underlying the Stac Fada Member at some locations (e.g., Second Coast) (Simms 2015), while we do not see evidence for disturbance of the surrounding sediments – which would be expected due to the high velocities of spall blocks (Oberbeck 1975; Melosh 1989) – we cannot rule out the possibility that these are isolated crater-derived blocks ejected and transported for considerable distances beyond the continuous ejecta blanket.

At most impact craters on Earth with preserved ejecta deposits, the continuous ejecta blanket is overlain by a second patchy layer of ejecta (Osinski *et al.* 2011). The properties of these overlying deposits are fundamentally different to the underlying continuous ejecta blankets. These overlying deposits are melt rich (being impact melt rocks and/or melt-bearing breccias, often termed suevite), contain a much higher proportion of shocked material, are still poorly sorted but do not contain clasts on the 10s m to km-scale, and are derived from deeper in the target stratigraphy (Osinski *et al.* 2011, 2012) (Table 1).

As outlined in Table 1 and shown in Figures 5 and 6, the Stac Fada Member also bears little to no resemblance to the melt-bearing ejecta deposits at the Ries and Mistastin impact structures – the two best-preserved examples on Earth – or other craters as described in Osinski *et al.* (2011). While these ejecta deposits contain more melt than continuous ejecta blankets like the Bunte Breccia at the Ries structure, and similar to the Stac Fada Member, there are several important differences. Most importantly, the Stac Fada Member is moderately to very well sorted, contains very few shocked mineral clasts, no shocked lithic clasts, is dominated by vitric clasts rather than lithic clasts, and possesses internal layering and grading, all properties that fundamentally differentiate this unit from all other documented melt-bearing ejecta deposits on Earth (Table 1; Figs. 5, 6). In summary, in contrast to previous suggestions (Amor *et al.* 2008; Branney & Brown 2011), the properties of the Stac Fada

Member are unlike any other confirmed proximal ejecta deposits on Earth. But what about Mars?

Several previous workers have drawn analogies between the Stac Fada Member and impact ejecta deposits on Mars (Amor *et al.* 2008; Simms 2015). This analogy was largely based on invoking an impact into volatile-rich target rocks. Unfortunately, the ancient and eroded nature of the Stac Fada Member does not allow for any quantitative comparision to be made with martian ejecta deposits via satellite imagery – such as has been made for the Ries impact structure for example (Sturm *et al.* 2013) – and the lack of samples or surface-based imagery from rovers or landers from the latter also precludes any direct comparision. However, based on a combination of theoretical and observational considerations, regardless of the complicating factors due to volatiles and/or an atmosphere on Mars (Barlow 2005), it is still predicted that single layer ejecta craters are initially emplaced ballistically (Osinski 2006; Oberbeck 2009), which as discussed above, appears incompatible with the properties of the Stac Fada Member.

6.3. Origin of the Stac Fada Member

Unlike the stark differences between the Stac Fada Member and continuous impact ejecta deposits, it shares many striking similarities with impact melt-bearing breccias of the Onaping Formation (Sudbury) and those at the Chicxulub impact structure are striking (Table 1; Figs. 5, 6). These include the predominance of vitric particles, low abundance of shocked material, overall well-sorted textures and presence of internal layering.

Long thought to be a fallback breccia (French 1967), the Onaping Formation has been reinterpreted as the product of melt-fuel-coolant interactions (MFCI; Grieve *et al.* 2010), a process similar to what occurs during phreatomagmatic volcanic eruptions or hydrovolcanism.

394 The products of volcanic MFCI activity are layered, fine-grained (fine to medium ash size),
395 well sorted, and glass is the most abundant clastic component (Büttner *et al.* 2002). In this
396 scenario, it is envisaged that seawater entered the Sudbury crater soon after the impact and
397 encountered the superheated impact melt sheet (i.e., the proto-Sudbury Igneous Complex). A
398 vapour film was created that would have expanded and collapsed rapidly as seawater came
399 into direct contact with the melt to generate repetitive melt quenching and fragmentation
400 (Wohletz 1983; Büttner *et al.* 2002; Grieve *et al.* 2010; Wohletz *et al.* 2013). The MFCI
401 model is consistent with the fact that Sudbury occurred in a marine setting and has been tested
402 via comparison with volcanic MFCI deposits (Osinski *et al.* 2016). Chicxulub impact melt-
403 bearing breccias share many of the same attributes as the Onaping Formation and an MFCI
404 origin for those has also been recently proposed (Osinski *et al.* 2020). It is worth mentioning
405 that various origins have been proposed for suevite at the Ries impact structure, including the
406 suggestion that MFCI played a role (Artemieva *et al.* 2013; Stöffler *et al.* 2013). However, as
407 is clear in Table 1 and as discussed by (Osinski *et al.* 2016) and Siegert *et al.* (2017), the Ries
408 suevites bear little to no resemblance to volcanic MFCI deposits, or the aforementioned
409 Sudbury and Chicxulub deposits, and thus do not share the same origin.
410 Intriguingly, the Stac Fada Member contains many of the features of the Onaping
411 Formation and Chicxulub impact melt-bearing breccias (Table 1), which hints strongly at
412 causality and an origin involving MFCI. There are some differences, but these are subtle. For
413 example, the vitric particles in the Stac Fada Member display a wider range of shapes and
414 higher abundance of vesicles and clastic material is also more abundant compared to Sudbury
415 or Chicxulub, but such differences are readily explained by variations of water-to-melt-mass
416 ratios (e.g., Wohletz 1983). What is more central to the discussion is palaeogeography. Both
417 the Onaping and Chicxulub deposits occur in the interior of large ~200–250 km diameter size
418 craters located on what were shallow-marine shelves at the time of impact; no crater or melt

material of comparable scale is known for the Stac Fada Member, which also does not sit inside a crater (as far as we know). Hence, we propose a modified MFCI scenario.

Our working hypothesis is underpinned by three observations: (i) the Stac Fada Member rests on a succession of fluvial sandstones variably many tens to several hundreds of metres thick; (ii) shocked quartz is predominantly in the form of mineral clasts – consistent with a sandstone protolith – and gneiss clasts are unshocked, evidence that the impact likely breached the supracrustal cover sequence but not the crustal rocks; and (iii) fluvial deposition resumed following the impact, as evident by the presence of sandstones identical to those of the Bay of Stoer Formation that reoccur between the top of the Stac Fada Member and the Poll a'Mhuilt estuarine mudstones. Further, given that the Poll a'Mhuilt Member contains evidence for marine influences on deposition (Stüeken *et al.* 2017), shallow-marine settings would have been nearby.

Our proposed scenario begins similar to that envisaged by Amor *et al.* (2008), namely that the impact was into volatile-rich sediments. However, the Stac Fada is encased by sandstone bodies that are identical to those that typify the underlying Bay-of-Stoer Formation (according to the revised stratigraphy of Simms 2015) and not, as suggested by Amor et al. (2008), the mudstones of the Poll a'Mhuilt. Hence, unlike their scenario, it is far more in keeping with the stratigraphic observations that the impact was into the river systems and water-laden sandy sediments that are now preserved as the Bay of Stoer Formation rather than the mudstones of the Poll a'Mhuilt. Hence, there would have been abundant water to drive MFCI within the host crater and to transport this melt and other crater-derived material well beyond the host crater. Indeed, using the Oruanui Formation of New Zealand – the product of a 27 ka phreatomagmatic eruption from the Taupo Volcanic Zone – as an example, MFCI deposits can extend several hundred km from their source and cover thousands of square kilometres (Self & Sparks 1978). This dispersal by such energetic interactions thus accounts

for the high amount of melt but also for the low amount of shocked material in the Stac Fada Member.

In keeping with the presence of sedimentary structures and properties in the Stac Fada Member similar to debris flows (e.g., Stewart 2002; Young 2002), mud flows (Simms 2015), and density currents (Branney & Brown 2011), we envisage that its sedimentation would have been outwith the extent of the continuous ballistically-emplaced ejecta blanket as high-energy ground-hugging sediment gravity flows. Such a scenario is consistent with the careful sedimentological work of Stewart (2002) and Young (2002) modified by the knowledge that the melt component was generated by hypervelocity impact rather than volcanism. Whether the emplacement of these flows was triggered by the deposition of impact ejecta elsewhere, the MFCI process itself, or due to seismic shaking initiated by the impact, remains to be determined. Whatever the trigger, it is clear that the emplacement of the Stac Fada Member was rapid given the restriction of accretionary lapilli and dust pellets – which would have formed in the ejecta plume (Branney & Brown 2011; Johnson & Melosh 2014) – in the upper parts of the sequence. As for the location of the impact crater, we remain agnostic and await with the hope that additional evidence will be found to determine its position (assuming that it is preserved).

7. Concluding remarks

The Stac Fada Member is unique within the Torridonian Supergroup of northwest Scotland and, unsurprisingly, has been the subject of much debate over the past 50 years or so. A significant advancement in our understanding of this unit was the discovery of shocked quartz grains and other isotopic and geochemical evidence for an impact origin by Amor *et al.* (2008). In this contribution we have confirmed the presence of shocked material in the Stac

Fada Member but highlight several properties that are clearly different to other known and well characterized impact ejecta deposits. As such, the Stac Fada Member should not be used to infer emplacement of impact ejecta in general (Branney & Brown 2011). We offer a modified impact model involving MFCI based on the similarities of the Stac Fada Member with well-sorted, glass-rich breccias from the Sudbury and Chicxulub impact structures and with volcanic MFCI deposits formed during phreatomagmatic volcanic eruptions.

In closing, we note that the Stac Fada Member deposits are not accounted for in the current proposed classification scheme for impactites (Stöffler & Grieve 2007). They are unquestionably not impact melt rocks as proposed by (Amor *et al.* 2019), which by definition possess an igneous groundmass (e.g., Dence 1971; Stöffler & Grieve 2007; Osinski *et al.* 2018). We have also shown that Stac Fada Member breccias bear little resemblance to traditional "suevite" found at craters such as the Ries and Mistastin impact structures. Instead, the Stac Fada Member joins the Onaping Formation at the Sudbury impact structure and the melt-bearing breccias at Chicxulub in representing a new class of impact product akin to volcaniclastic rocks (cf., Osinski *et al.* 2020).

Acknowledgements This paper is dedicated to Grant Young who sadly passed away in August 2020. Grant was a long standing member of the Department of Earth Sciences at Western. During his long career he made numerous important contributions to understanding the geology of the Scottish Highlands, including the Stac Fada Member. We also thank Richard A. F. Grieve for discussions on this topic, Stephen Wood for preparation of the thin sections, and John Ferries for his companionship in the field. Michael Simms, Ken Amor, and an anonymous reviewer are thanked for their thoughtful and constructive reviews on this manuscript.

Funding Funding to GRO. from the Natural Sciences and Engineering Research Council of Canada (NSERC) Discovery Grant program and the Canadian Space Agency (CSA) Canadian Analogue Research Network and Field Investigation programs is gratefully acknowledged. Part of LF's work was supported by the Department of Foreign Affairs and International Trade (DFAIT), Government of Canada.

Author contributions GRO: conceptualization (lead), formal analysis (lead), funding acquisition (lead), investigation (lead), methodology (lead), project administration (lead), resources (lead), supervision (lead), validation (lead), visualization (lead), writing – original draft (lead), writing – review and editing (lead). LF: formal analysis (supporting), investigation (supporting), methodology (supporting), validation (supporting), visualization (supporting), writing – original draft (supporting), writing – review and editing (supporting). PJAH: formal analysis (supporting), investigation (supporting), methodology (supporting), validation (supporting), visualization (supporting), writing – review and editing (supporting). ARP: investigation (supporting), writing – review and editing (supporting). LJP: investigation (supporting), writing – review and editing (supporting). AS: investigation (supporting), writing – review and editing (supporting). AEP: investigation (supporting), writing – review and editing (supporting).

Data Access Statement Most data generated or analysed during this study are included in this published article. Additional raw data are available from the corresponding author on reasonable request.

References

Ames, D.E., Golightly, J.P., Lightfoot, P.C. & Gibson, H.L. 2002. Vitric compositions in the

519 Onaping Formation and their relationship to the Sudbury Igneous Complex, Sudbury
520 Structure. *Economic Geology*, **97**, 1541–1562.

521 Ames, D.E., Davidson, A. & Wodicka, N. 2008. Geology of the giant Sudbury polymetallic
522 mining camp, Ontario, Canada. *Economic Geology*, **103**, 1057–1077.

523 Amor, K., Hesselbo, S.P., Porcelli, D., Thackrey, S. & Parnell, J. 2008. A Precambrian
524 proximal ejecta blanket from Scotland. *Geology*, **36**, 303–306.

525 Amor, K., Hesselbo, S.P., et al. 2019. The Mesoproterozoic Stac Fada proximal ejecta
526 blanket, NW Scotland: constraints on crater location from field observations, anisotropy
527 of magnetic susceptibility, petrography and geochemistry. *Journal of the Geological*
528 *Society*, **176**, 830–846, https://doi.org/10.1144/jgs2018-093.

529 Artemieva, N.A., Wünnemann, K., Krien, F., Reimold, W.U. & Stöffler, D. 2013. Ries crater
530 and suevite revisited—Observations and modeling Part II: Modeling. *Meteoritics &*
531 *Planetary Science*, **48**, 515–589, https://doi.org/10.1111/maps.12085.

532 Barlow, N.G. 2005. A review of martian impact crater ejecta structrues and their implications
533 for target properties. *In*: Kenkmann, T., Hörz, F. & Deutsch, A. (eds) *Large Meteorite*
534 *Impacts III: Geological Society of America Special Paper 384*. Boulder, Geological
535 Society of America, 433–442.

536 Branney, M.J. & Brown, R.J. 2011. Impactoclastic density current emplacement of terrestrial
537 meteorite-impact ejecta and the formation of dust pellets and accretionary lapilli:
538 Evidence from Stac Fada, Scotland. *The Journal of Geology*, **119**, 275–292.

539 Butler, R.W.H. & Alsop, I. 2019. A reassessment of the proposed 'Lairg Impact Structure'
540 and its potential implications for the deep structure of northern Scotland: a discussion.
541 *Journal of the Geological Society*, **177**, 443–446, https://doi.org/10.1144/jgs2019-168.

542 Büttner, R., Dellino, P., La Volpe, L., Lorenz, V. & Zimanowski, B. 2002. Thermohydraulic

explosions in phreatomagmatic eruptions as evidenced by the comparison between pyroclasts and products from Molten Fuel Coolant Interaction experiments. *Journal of Geophysical Research: Solid Earth*, **107**, doi:10.1029/2001JB000511.

Chanou, A., Osinski, G.R. & Grieve, R.A.F. 2014. A methodology for the semi-automatic digital image analysis of fragmental impactites. *Meteoritics & Planetary Science*, **49**, 621–635, https://doi.org/10.1111/maps.12267.

Christeson, G.L., Gulick, S.P.S., et al. 2018. Extraordinary rocks from the peak ring of the Chicxulub impact crater: P-wave velocity, density, and porosity measurements from IODP/ICDP Expedition 364. *Earth and Planetary Science Letters*, **495**, 1–11, https://doi.org/https://doi.org/10.1016/j.epsl.2018.05.013.

Dence, M.R. 1971. Impact melts. *Journal of Geophysical Research*, **76**, 5552–5565.

Drake, S.M., Beard, A.D., et al. 2017. Discovery of a meteoritic ejecta layer containing unmelted impactor fragments at the base of Paleocene lavas, Isle of Skye, Scotland. *Geology*, **46**, 171–174, https://doi.org/10.1130/G39452.1.

Emmons, R.C. 1943. *The Universal Stage (with Five Axes of Rotation), Geological Society of America Memoir 8*. Boulder, Geological Society of America.

Engelhardt, W. v. & Bertsch, W. 1969. Shock induced planar deformation structures in quartz from the Ries crater, Germany. *Contributions to Mineralogy and Petrology*, **20**, 203–234.

Engelhardt, W. v. 1990. Distribution, petrography and shock metamorphism of the ejecta of the Ries crater in Germany - a review. *Tectonophysics*, **171**, 259–273.

Engelhardt, W. v. 1997. Suevite breccia of the Ries impact crater, Germany: Petrography, chemistry and shock metamorphism of crystalline rock clasts. *Meteoritics & Planetary Science*, **32**, 545–554.

567 Engelhardt, W. v & Graup, G. 1984. Suevite of the Ries crater, Germany: Source rocks and
568 implications for cratering mechanics. *Geologische Rundschau*, **73**, 447–481.

569 Ferrière, L. & Osinski, G.R. 2012. Shock Metamorphism. *In*: Osinski, G. R. & Pierazzo, E.
570 (eds) *Impact Cratering: Processes and Products*. Chichester, Wiley-Blackwell, 106–124.

571 Ferrière, L., Koeberl, C., Ivanov, B.A. & Reimold, W.U. 2008. Shock Metamorphism of
572 Bosumtwi Impact Crater Rocks, Shock Attenuation, and Uplift Formation. *Science*, **322**,
573 1678–1681, https://doi.org/10.1126/science.1166283.

574 Ferrière, L., Morrow, J.R., Amgaa, T. & Koeberl, C. 2009a. Systematic study of universal-
575 stage measurements of planar deformation features in shocked quartz: Implications for
576 statistical significance and representation of results. *Meteoritics & Planetary Science*, **44**,
577 925–940.

578 Ferrière, L., Koeberl, C., Reimold, W.U., Hecht, L. & Bartosova, K. 2009b. The origin of
579 “toasted” quartz in impactites revisited. *Lunar and Planetary Science Conference*, **40**,
580 1751 pdf.

581 French, B.M. 1967. Sudbury Structure, Ontario: Some petrographic evidence for origin by
582 meteorite impact. *Science*, **156**, 1094–1098,
583 https://doi.org/10.1126/science.156.3778.1094.

584 French, B.M. & Koeberl, C. 2010. The convincing identification of terrestrial meteorite
585 impact structures: What works, what doesn’t, and why. *Earth-Science Reviews*, **98**, 123–
586 170.

587 Gracie, A.J. & Stewart, A.D. 1967. Torridonian sediments at Enard Bay, Ross-shire. *Scottish*
588 *Journal of Geology*, **3**, 181 LP – 194, https://doi.org/10.1144/sjg03020181.

589 Grieve, R.A.F. 2017. Logan Medallist 4. Large-Scale Impact and Earth History. *Geoscience*
590 *Canada; Volume 44, Number 1 (2017)DO - 10.12789/geocanj.2017.44.113*.

591 Grieve, R.A.F., Ames, D.E., Morgan, J. V & Artemieva, N. 2010. The evolution of the
592 Onaping Formation at the Sudbury impact structure. *Meteoritics & Planetary Science*,
593 **45**, 759–782, https://doi.org/10.1111/j.1945-5100.2010.01057.x.

594 Hill, P.J.A., Osinski, G.R. & Banerjee, N.R. 2020. Through the impact glass: Insight into the
595 evolution of melt at the Mistastin Lake impact structure. *Meteoritics & Planetary*
596 *Science*, doi:10.1111/maps.13457, https://doi.org/10.1111/maps.13457.

597 Hörz, F. 1968. Statistical measurements of deformation structures and refractive indices in
598 experimentally shock loaded quartz. *In*: French, B. M. & Short, N. M. (eds) *Shock*
599 *Metamorphism of Natural Materials*. Baltimore, Mono Book Corporation, 243–253.

600 Hörz, F. 1982. Ejecta of the Ries Crater, Germany. *In*: Silver, L. T. & Schultz, P. H. (eds)
601 *Geological Implications of Impacts of Large Asteroids and Comets on the Earth,*
602 *Geological Society of America Special Paper 190*. Boulder, Colorado, USA, Geological
603 Society of America, 39–55.

604 Hörz, F., Ostertag, R. & Rainey, D.A. 1983. Bunte breccia of the Ries: Continuous deposits of
605 large impact craters. *Reviews of Geophysics and Space Physics*, **21**, 1667–1725.

606 Huber, M.S., Ferrière, L., Losiak, A. & Koeberl, C. 2011. ANIE: A mathematical algorithm
607 for automated indexing of planar deformation features in quartz grains. *Meteoritics &*
608 *Planetary Science*, **46**, 1418–1424, https://doi.org/10.1111/j.1945-5100.2011.01234.x.

609 Huffman, A.R. & Reimold, W.U. 1996. Experimental constraints on shock-induced
610 microstructures in naturally deformed silicates. *Tectonophysics*, **256**, 165–217,
611 https://doi.org/https://doi.org/10.1016/0040-1951(95)00162-X.

612 Johnson, B.C. & Melosh, H.J. 2014. Formation of melt droplets, melt fragments, and
613 accretionary impact lapilli during a hypervelocity impact. *Icarus*, **228**, 347–363,
614 https://doi.org/10.1016/j.icarus.2013.10.022.

615 Kenny, G.G., O'Sullivan, G.J., Alexander, S., Simms, M.J., Chew, D.M. & Kamber, B.S.
616 2019. On the track of a Scottish impact structure: a detrital zircon and apatite provenance
617 study of the Stac Fada Member and wider Stoer Group, NW Scotland. *Geological*
618 *Magazine*, **156**, 1863–1876, https://doi.org/DOI: 10.1017/S0016756819000220.

619 Lawson, D.E. 1973. Torridonian volcanic sediments. *Scottish Journal of Geology*, **8**, 345 LP –
620 362, https://doi.org/10.1144/sjg08040345.

621 Mader, M.M. & Osinski, G.R. 2018. Impactites of the Mistastin Lake impact structure:
622 Insights into impact ejecta emplacement. *Meteoritics & Planetary Science*, **53**, 2492–
623 2518.

624 Melosh, H.J. 1989. *Impact Cratering: A Geologic Process*. New York, Oxford University
625 Press.

626 Muir, T.L. & Peredery, W.V. 1984. The Onaping Formation. *In*: Pye, E. G., Naldrett, A. J. &
627 Giblin, P. E. (eds) *The Geology and Ore Deposits of the Sudbury Structure, Ontario*
628 *Geological Survey Special Volume 1*. Toronto, Ministry of Natural Resources, 139–210.

629 Müller, W.F. & Défourneaux, M. 1968. Deformationsstrukturen im Quarz als Indikator für
630 Stosswellen: Eine experimentelle Untersuchung an Quartz-Einkristallen. *Geophysik*, **34**,
631 483–504.

632 Oberbeck, V.R. 1975. The role of ballistic erosion and sedimentation in lunar stratigraphy.
633 *Reviews of Geophysics and Space Physics*, **13**, 337–362.

634 Oberbeck, V.R. 2009. Layered ejecta craters and the early water/ice aquifer on Mars.
635 *Meteoritics & Planetary Science*, **44**, 43–54, https://doi.org/10.1111/j.1945-
636 5100.2009.tb00716.x.

637 Osinski, G.R. 2006. Effect of volatiles and target lithology on the generation and
638 emplacement of impact crater fill and ejecta deposits on Mars. *Meteoritics & Planetary*

639 *Science*, **41**, 1571–1586.

640 Osinski, G.R. & Grieve, R.A.F. 2019. Impact Earth: A new resource for outreach, teaching,
641 and research. *Elements*, **15**, 70–71.

642 Osinski, G.R. & Pierazzo, E. 2012. *Impact Cratering: Processes and Products*. Wiley-
643 Blackwell.

644 Osinski, G.R., Grieve, R.A.F. & Spray, J.G. 2004. The nature of the groundmass of surficial
645 suevites from the Ries impact structure, Germany, and constraints on its origin.
646 *Meteoritics & Planetary Science*, **39**, 1655–1684.

647 Osinski, G.R., Tornabene, L.L. & Grieve, R.A.F. 2011. Impact ejecta emplacement on the
648 terrestrial planets. *Earth and Planetary Science Letters*, **310**, 167–181.

649 Osinski, G.R., Grieve, R.A.F. & Tornabene, L.L. 2012. Excavation and impact ejecta
650 emplacement. *In*: Osinski, G. R. & Pierazzo, E. (eds) *Impact Cratering: Processes and*
651 *Products*. Chichester, Wiley-Blackwell, 43–59.

652 Osinski, G.R., Grieve, R.A.F., Chanou, A. & Sapers, H.M. 2016. The "suevite" conundrum,
653 Part 1: The Ries suevite and Sudbury Onaping Formation compared. *Meteoritics and*
654 *Planetary Science*, **51**, 2316–2333, https://doi.org/10.1111/maps.12728.

655 Osinski, G.R., Grieve, R.A.F., Bleacher, J.M., Neish, C.D., Pilles, E.A. & Tornabene, L.L.
656 2018. Igneous rocks formed by hypervelocity impact. *Journal of Volcanological and*
657 *Geothermal Research*, **353**, 25–54.

658 Osinski, G.R., Grieve, R.A.F., et al. 2020. Explosive interaction of impact melt and seawater
659 following the Chicxulub impact event. *Geology*, **48**, 108–112,
660 https://doi.org/10.1130/G46783.1.

661 Parnell, J., Mark, D., Fallick, A.E., Boyce, A. & Thackrey, S. 2011. The age of the
662 Mesoproterozoic Stoer Group sedimentary and impact deposits, NW Scotland. *Journal*

663 *of the Geological Society*, **168**, 349–358, https://doi.org/10.1144/0016-76492010-099.

664 Reddy, S.M., Johnson, T.E., Fischer, S., Rickard, W.D.A. & Taylor, R.J.M. 2015.
665 Precambrian reidite discovered in shocked zircon from the Stac Fada impactite, Scotland.
666 *Geology*, **43**, 899–902, https://doi.org/10.1130/G37066.1.

667 Sanders, I.S. & Johnston, J.D. 1989. The Torridonian Stac Fada Member: an extrusion of
668 fluidised peperite? *Transactions of the Royal Society of Edinburgh: Earth Sciences*, **80**,
669 1–4, https://doi.org/DOI: 10.1017/S0263593300012220.

670 Self, S. & Sparks, R.S.J. 1978. Characteristics of widespread pyroclastic deposits formed by
671 the interaction of silicic magma and water. *Bulletin Volcanologique*, **41**, 196–212,
672 https://doi.org/10.1007/BF02597223.

673 Shoemaker, E.M. 1963. Impact mechanics at Meteor Crater, Arizona. *In*: Middlehurst, B. M.
674 & Kuiper, G. P. (eds) *The Moon, Meteorites and Comets*. Illinois, University of Chicago
675 Press, 301–336.

676 Siegert, S., Branney, M.J. & Hecht, L. 2017. Density current origin of a melt-bearing impact
677 ejecta blanket (Ries suevite, Germany). *Geology*, **45**, 855–858.

678 Simms, M.J. 2015. The Stac Fada impact ejecta deposit and the Lairg Gravity Low: evidence
679 for a buried Precambrian impact crater in Scotland? *Proceedings of the Geologists'*
680 *Association*, **126**, 742–761, https://doi.org/https://doi.org/10.1016/j.pgeola.2015.08.010.

681 Simms, M.J. 2019. Reply to Discussion on 'A reassessment of the proposed "Lairg Impact
682 Structure" and its potential implications for the deep structure of northern Scotland'.
683 *Journal of the Geological Society*, jgs2019-186, https://doi.org/10.1144/jgs2019-186.

684 Simms, M.J. & Ernstson, K. 2019. A reassessment of the proposed 'Lairg Impact Structure'
685 and its potential implications for the deep structure of northern Scotland. *Journal of the*
686 *Geological Society*, https://doi.org/10.1144/jgs2017-161.

687 Stewart, A.D. 2002. *The Later Proterozoic Torridonian Rocks of Scotland: Their*
688 *Sedimentology, Geochemistry and Origin*. London, The Geological Society of London.

689 Stöffler, D. 1972. Deformation and transformation of rock-forming minerals by natural and
690 experimental shock processes: I. Behavior of minerals under shock compression.
691 *Fortschritte der Mineralogie*, **49**, 50–113.

692 Stöffler, D. 1984. Glasses formed by hypervelocity impact. *Journal of Non-Crystalline Solids*,
693 **67**, 465–502.

694 Stöffler, D. & Grieve, R.A.F. 2007. Impactites. *In*: Fettes, D. & Desmons, J. (eds)
695 *Metamorphic Rocks*. Cambridge, Cambridge University Press, 82–92.

696 Stöffler, D. & Langenhorst, F. 1994. Shock metamorphism of quartz in nature and
697 experiment: 1. Basic observation and theory. *Meteoritics*, **29**, 155–181.

698 Stöffler, D., Artemieva, N.A., Wünnemann, K., Reimold, W.U., Jacob, J., Hansen, B.K. &
699 Summerson, I.A.T. 2013. Ries crater and suevite revisited—Observations and modeling
700 Part I: Observations. *Meteoritics & Planetary Science*, **48**, 515–589.

701 Stüeken, E.E., Bellefroid, E.J., Prave, A., Asael, D., Planavsky, N.J. & Lyons, T.W. 2017.
702 Not so non-marine? Revisiting the Stoer Group and the Mesoproterozoic biosphere.
703 *Geochemical Perspectives Letters*, **3**, 221–229,
704 https://doi.org/http://dx.doi.org/10.7185/geochemlet.1725.

705 Sturm, S., Wulf, G., Jung, D. & Kenkmann, T. 2013. The Ries impact, a double-layer rampart
706 crater on Earth. *Geology* , **41**, 531–534, https://doi.org/10.1130/G33934.1.

707 Walkden, G., Parker, J. & Kelley, S. 2002. A Late Triassic Impact Ejecta Layer in
708 Southwestern Britain. *Science*, **298**, 2185–2188.

709 Whitehead, J., Spray, J.G. & Grieve, R.A.F. 2002. Origin of 'toasted' quartz in terrestrial
710 impact structures. *Geology*, **30**, 431–434.

Wohletz, K.H. 1983. Mechanisms of hydrovolcanic pyroclast formation: Grain-size, scanning electron microscopy, and experimental studies. *Journal of Volcanology and Geothermal Research*, **17**, 31–63, https://doi.org/http://dx.doi.org/10.1016/0377-0273(83)90061-6.

Wohletz, K.H., Zimanowski, B. & Buttner, R. 2013. Magma-water interactions. *In*: Fagents, S. A., Gregg, T. K. P. & Lopes, R. M. C. (eds) *Modeling Volcanic Processes: The Physics and Mathematics of Volcanism*. Cambridge University Press, 230–257.

Young, G.M. 2002. Stratigraphy and geochemistry of volcanic mass flows in the Stac Fada Member of the Stoer Group, Torridonian, NW Scotland. *Transactions: Earth Sciences*, **93**, 1–16.

Table 1. Basic characteristics of the Stac Fada Member, compared with Ries and Mistastin "suevite", the Sudbury Onaping Formation, and Chicxulub impact melt-bearing breccias from the International Ocean Discovery Program / International Continental Scientific Drilling Program Expedition 364, site M0077A (21.45° N, 89.95° W). Table expanded from Osinski et al. (2020).

	Ries (Engelhardt & Graup 1984; Engelhardt 1997; Osinski *et al.* 2004)	Mistastin (Mader & Osinski 2018)	Chicxulub (Osinski *et al.* 2020)	Sudbury (Muir & Peredery 1984; Ames *et al.* 2002, 2008; Grieve *et al.* 2010)	Stac Fada (this study and as noted)
Stratigraphy	No internal stratigraphy	No internal stratigraphy	Internal lithologies; layered on mm to dm-scale	Internal lithologies; layered	Internal lithologies; layered on mm to dm-scale (cf., Gracie and Stewart 1967; Simms 2015).

Relationship to topography	Deposits infill topography	Deposits infill topography	Deposits drape topography (Christeson *et al.* 2018)	Deposits drape topography	Deposits infill and drape topography (Stewart 2002; Simms 2015).
Sorting	Poorly to very poorly sorted	Poorly to very poorly sorted	Well to very well sorted	Well to very well sorted	Moderately to very well sorted
Graded?	No	No	Yes	Yes	Yes
Vitric clasts:					
Vol. %	Average 16 vol% (although finer fraction of the groundmass also has glass particles)	Average 15–20 vol%	>50 vol%	>60 vol%; up to 80 vol% in the Sandcherry Formation	Typically >55 vol%
Size	Typically 1–10 cm, but up to 1 m long in places	Typically 1–10 cm, but up to 0.8 m long in places	Typically 100s μm to ~5 mm; rarely > 1 cm	Typically 100s μm to 1–5 mm; rarely > 1 cm	Typically 100s μm to 1–5 mm; rarely > 1 cm (cf., Amor *et al.* 2008; Simms 2015).
Shape	Irregular	Irregular	Regular, equant	Regular, equant	Regular, equant
Alignment?	Yes	Yes	No	No	No to Rare
Mineral/ lithic fragments in clasts?	Abundant	Abundant	Rare	Rare	Rare
Vesicles?	Abundant	Abundant	Rare	Rare	Variable
Schlieren?	Abundant	Abundant	Rare	None/rare	None/rare
Quench crystallites?	Abundant	Abundant	None/rare	None	None
Impact melt rock clasts?	None	None	Yes	Yes	None
Deposition temperature	High (>900 ºC)	High (>900 ºC)	Low (<580 ºC)	Low	Low (~200 ºC) (Parnell *et al.* 2011)
Shock level of lithic clasts	>90 % shocked to > 10 GPa	>75 % shocked to > 10 GPa	<<5 % shocked	<<5 % shocked	<<5 % shocked

730

Table 2. Characteristics of quartz grains and main petrographic observations as determined by optical microscopy on 26 thin sections of the different types of breccia samples from the Bay of Stoer.

	UTM Coordinates	PFs	PDFs				Decorated PFs/PDFs	Notes
			1 set	2 sets	3 sets	4 sets		
Impact melt-bearing breccia								
SF08 002A	NC 03327 28532	1	3				4	Kink bands in muscovite
SF08 002B	NC 03327 28532	1	1	1	1			-
SF08 003A	NC 03330 28545	1	3	1	1		3	Kink bands in muscovite
SF08 003B	NC 03330 28545	1	3	1			1	One quartz grain with two PDF sets occurs within a vitric melt clast.
SF08 004A	NC 03323 28533		1	2			2	Kink bands in muscovite and rarely in feldspar grains
SF08 004B	NC 03323 28533	1	3	2			1	-
SF08 005A	NC 03317 28548	1	1	2	2	2	2	A few toasted quartz grains occur
SF08 005B	NC 03317 28548	1	4	2			1	Occurrence of a very vitric clast containing abundant undigested mineral clasts (mainly quartz but also a few feldspar grains).
SF08 005C	NC 03317 28548		2		1			Presence of shard-like vitric clasts
SF08 010A*	NC 03107 14582							Occurrence of vitric clasts recrystallized/altered to chlorite and zeolite
SF08 010B	NC 03107 14582		3	1	1		2	One quartz grain with one set of highly decorated PDF occurs within a vitric clasts. The thin section displays a large amount of vesicular vitric clasts
SF08 011	NC 03107 14582		2	1			1	Several highly fractured feldspar grains occur
SF08 012A	NC 03130 14598		1				1	-
SF08 012B*	NC 03130 14598							Several toasted quartz grains occur. Kink bands in muscovite. Many altered vitric clasts with numerous undigested angular quartz grains
Impact melt-bearing breccia with lapilli								
SF08 009A	NC 03081 14593	1	1					Presence of lapilli; the two shocked quartz grains occur within a lapilli
SF08 009B	NC 03081 14593		2				2	Presence of lapilli
Other type of breccia								
SF08 001A	NC 03326 28530	2	1					Kink bands in micas. No melt particles occur.
SF08 001B	NC 03326 28530	4	1				1	Kink bands in micas. No melt particles occur.

(*) Samples in which shocked quartz were not detected during our investigations.

Table 3. PDF set abundances and indexed PDF crystallographic orientations in quartz grains from 16 thin sections of breccia samples from the Bay of Stoer, as determined using the universal-stage.

No. of investigated grains	48
No. of measured sets	78
No. of PDF sets/grain (N)	1.6
PDF sets; % relative to total no. of quartz grains examined	
1 set	60
2 sets	21
3 sets	15
4 sets	4
Total	100
Indexed PDF crystallographic orientations; absolute frequency (%)[a]	
PDF crystallographic orientations	
c (0001)	3.8
$\{10\bar{1}4\}$	14.1
$\{10\bar{1}4\}$ // $\{10\bar{1}3\}$[b]	17
ω $\{10\bar{1}3\}$[c]	46
π $\{10\bar{1}2\}$	14
r, z $\{10\bar{1}1\}$	n.d.
m $\{10\bar{1}0\}$	n.d.
ξ $\{11\bar{2}2\}$	n.d.
s $\{11\bar{2}1\}$	n.d.
ρ $\{21\bar{3}1\}$	2.6
x $\{51\bar{6}1\}$	n.d.
a $\{11\bar{2}0\}$	n.d.
$\{22\bar{4}1\}$	1.3
$\{31\bar{4}1\}$	n.d.
t $\{40\bar{4}1\}$	n.d.
k $\{51\bar{6}0\}$	n.d.
Unindexed	1.3
Total	100

[a]Method described in Ferrière *et al.* (2009a); indexing done using the Automated Numerical Index Executor program (using the average value of measurements and a 5° error; see Huber *et al.* 2011).
[b]PDF planes which plot in the overlapping zone between $\{10\bar{1}4\}$ and $\{10\bar{1}3\}$ crystallographic orientations.
[c]$\{10\bar{1}3\}$ PDF orientations uniquely indexed.
n.d. = none detected.

Figure captions

Fig. 1. Simplified map of NW Scotland highlighting the location of the Stoer Group in red. The 5 study locations, from north to south, are Bay of Stoer (BS), Enard Bay (EB), Achiltibuie (A), Cailleach Head (CH), and Stattic Point (SP). Other abbreviations: MF = Minch Fault; MMH = Mid-Minch High; MTZ = Moine Thrust Zone; OHFZ = Outer Hebrides Fault Zone.

Fig. 2. Field photographs of the Stac Fada Member. (**a**) Bay of Stoer locality. (**b**) Same image as (**a**) with the Stac Fada Member highlighted in a red overlay. "SF2" and "SF4" correspond to the units of Young (2002) (see text for further details). "c" are two large sandstone clasts. (**c**) Classic example of the Stac Fada Member with green vitric clasts. Tip of rock hammer for scale. Bay of Stoer locality. (**d**) Rounded gneiss clast, centre above 35 cm-long rock hammer. Bay of Stoer locality. (**e**) The upper contact of the Stac Fada Member with overlying basal sandstones preserves evidence for erosion and reworking. (**f**) Accretionary lapilli at the Enard Bay locality. (**g**) Rock hammer resting on Stac Fada Member. The more rubbly outcrop wrapping around the "intact" Stac Fada Member is interpreted to be later channel fill deposits.

Fig. 3. Scanned polished thin sections of the Stac Fada Member melt-bearing breccias. All scale bars are 0.5 cm and all samples are from the Bay of Stoer locality.

Fig. 4. Plane-polarized light photomicrographs of the Stac Fada Member melt-bearing breccias. (**a**) Shard-like, devitrified and altered melt fragment from Bay of Stoer. Note the presence of quartz mineral clasts (**b**) Devitrified and altered melt fragment from Bay of Stoer. Note the elongated shape of the large vesicle. (**c**) Devitrified and altered melt fragment with vesicles infilled with the same phase that altered the glass (white arrows). Bay of Stoer locality. (**d**) Accretionary lapilli-rich sample from Enard Bay. Note the presence of whole and broken lapilli. Some lapilli have glass fragments in their cores (white arrows).

Fig. 5. Scanned hand specimen images and corresponding black and white image analysis products highlighting impact glass from the Stac Fada Member (**a**), Ries impact structure (Germany) (**b**), Mistastin Lake impact structure (Canada) (**c**), and the Onaping Formation of the Sudbury impact structure (Canada) (**d**). All scale bars are 1 cm.

Fig. 6. Cumulative area and perimeter fraction plots to show the degree of sorting in Stac Fada Member and other impact melt-bearing breccia deposits. Here the cumulative area fraction is a running total of the area for particles of interest over the total area for all particles of interest. Likewise, the cumulative perimeter fraction is a running total of the perimeter for particles of interest over the total perimeter for all particles of interest. (**a**) Using the methods of Chanou et al. (2014), the results for a typical sorting scale clearly differentiate each sorting. The slope indicates the rate of fraction increase which is greater for poorly sorted samples. The cut-offs and jumps in the fractions are due to the occurrence of larger and more complex particles causing a shift in the cumulative values. The results for a typical sorting scale clearly differentiate each sorting level. Very well-sorted samples have a slope of ~1 and show a continuous linear distribution. Less sorted samples have progressively steeper and more discontinuous distributions. (**b**) Results for the Stac Fada Member demonstrate the high degree of sorting. (**c**) Traditional "suevite" from the Ries and Mistastin Lake impact structures (see Figs. 5b and c) are clearly more poorly sorted than the Stac Fada Member. (**d**) The Onaping Formation (see Fig. 5d) from the Sudbury impact structure and impact melt-bearing breccias from the Chicxulub impact structure (from IODP/ICDP Expedition 364, site M0077A) are well sorted, like the Stac Fada Member.

Fig. 7. Thin section photomicrographs (in cross-polarized light) of shocked quartz grains in breccia samples from the Stac Fada Member. (**a**) Large toasted quartz grain with the typical orange-brown to grayish-reddish brown appearance (sample 012b). (**b**) Quartz grain with one prominent set of c(0001) planar fractures (PF) (sample 001b). (**c**) Quartz grain containing two decorated PDF sets with $\omega\{10\bar{1}3\}$-equivalent orientations (sample 010b). (**d**) Small quartz grain with two sets of decorated PDFs; both PDF sets with $\omega\{10\bar{1}3\}$-equivalent orientations (sample 004a). (**e**) Highly shocked quartz grain with three PDF sets, with $\omega\{10\bar{1}3\}$-, $\{10\bar{1}4\}$-, and $\omega'\{01\bar{1}3\}$-equivalent orientations (sample 002b). (**f**) Quartz grain showing one prominent decorated PDF set with $\omega\{10\bar{1}3\}$-equivalent orientation. Note that another PDF set (*), with $\pi\{10\bar{1}2\}$-equivalent orientation, is visible in this grain under U-stage microscope (sample 004a).

Fig. 8. Histogram of the absolute frequency percent of indexed PDFs in quartz grains from Stac Fada breccia samples using the Automated Numerical Index Executor (ANIE) program (with the average value of measurements and a 5° error; see Huber et al., 2011) for the indexing. Note that PDF planes that fall into the overlap zone between $\{10\bar{1}4\}$ and $\{10\bar{1}3\}$

crystallographic orientations (see Table 3) are considered as $\{10\bar{1}3\}$ orientations in this figure, as suggested by (Ferrière *et al.* 2009a).

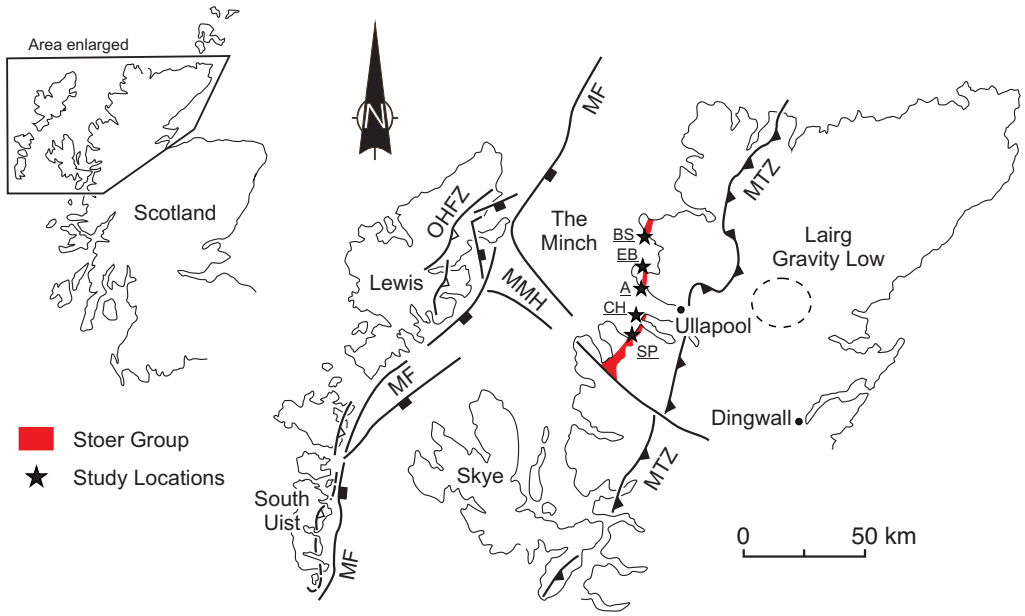
Area enlarged
Scotland
Stoer Group
Study Locations
N
OHFZ
MF
MMH
MF
MF
MF
MTZ
MTZ
Lewis
The
Minch
BS
EB
A
CH
SP
Ullapool
Lairg
Gravity Low
Dingwall
Skye
South
Uist
0
50 km

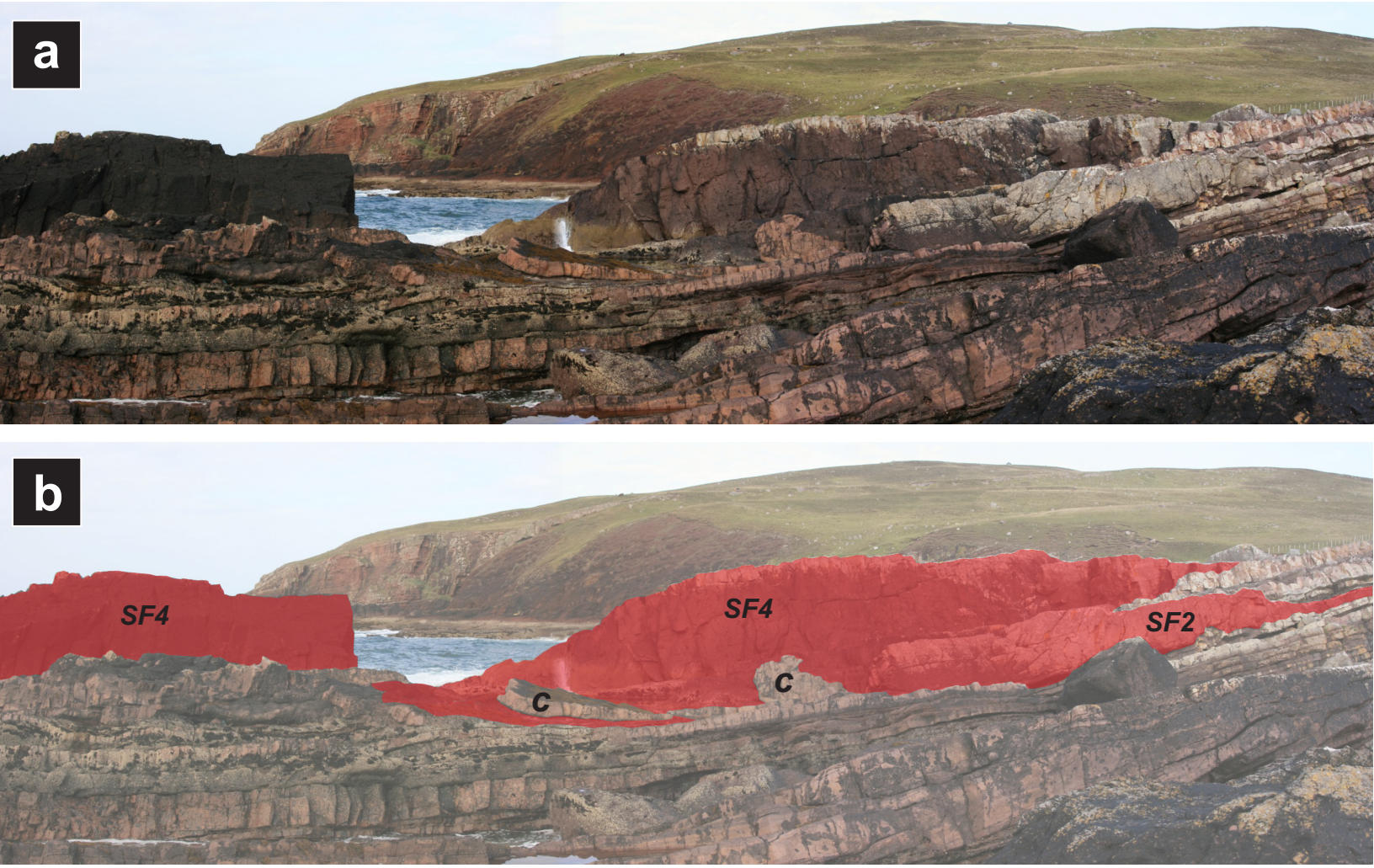
a

b
SF4
SF4
SF2
c
c

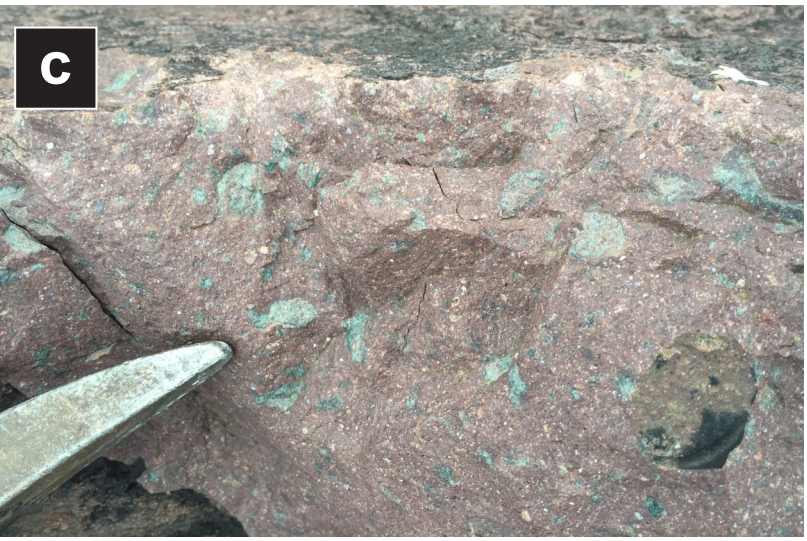
c


d


e


f

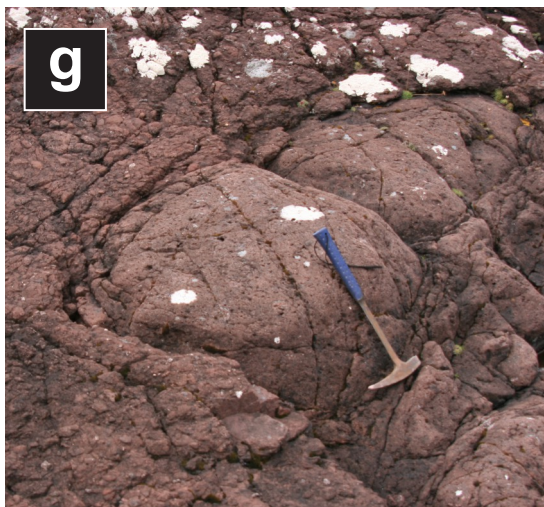
g

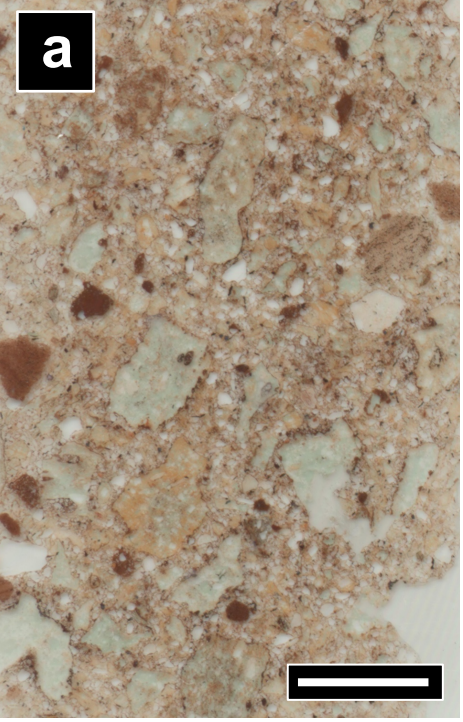
a


b

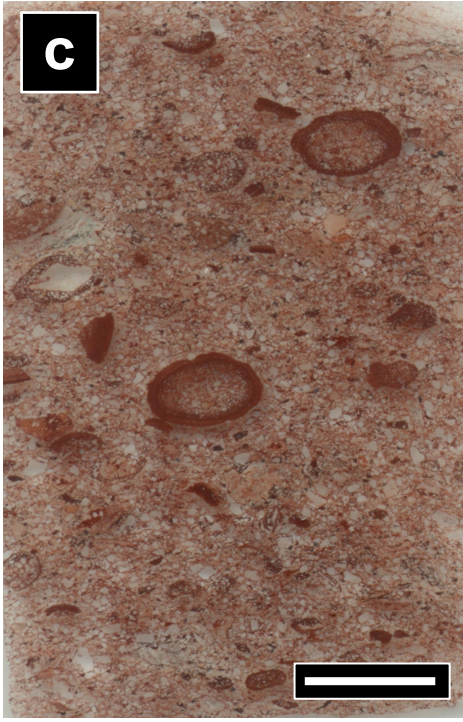
c

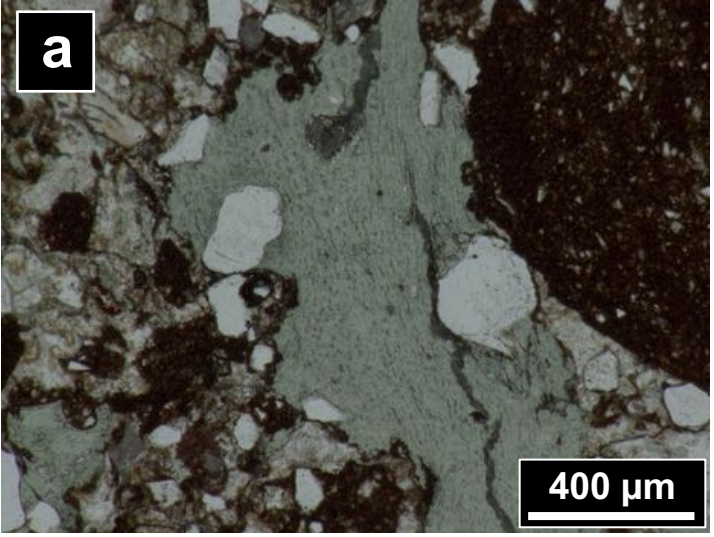
a
400 µm

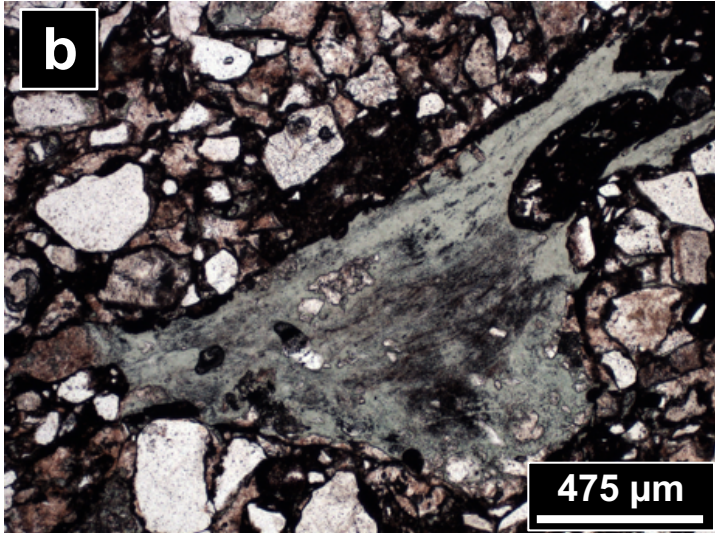
b
475 µm

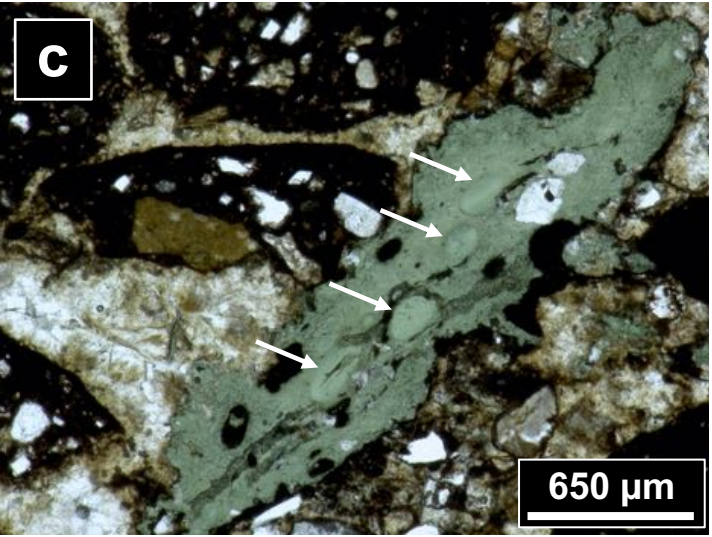
c
650 µm

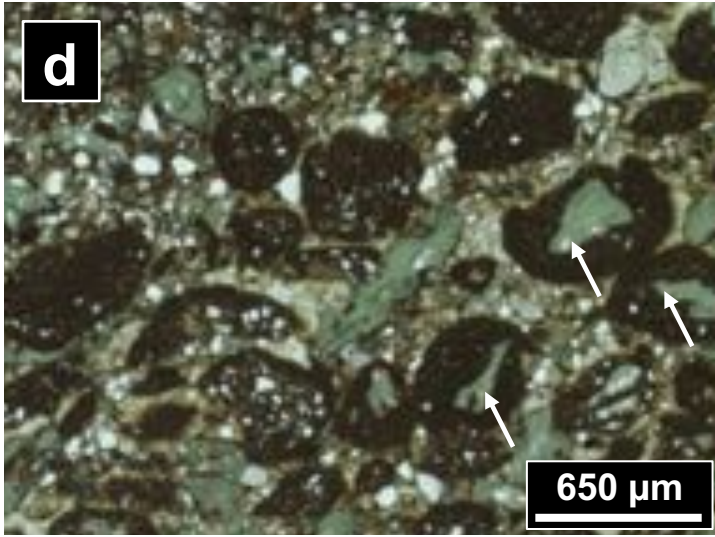
d
650 µm

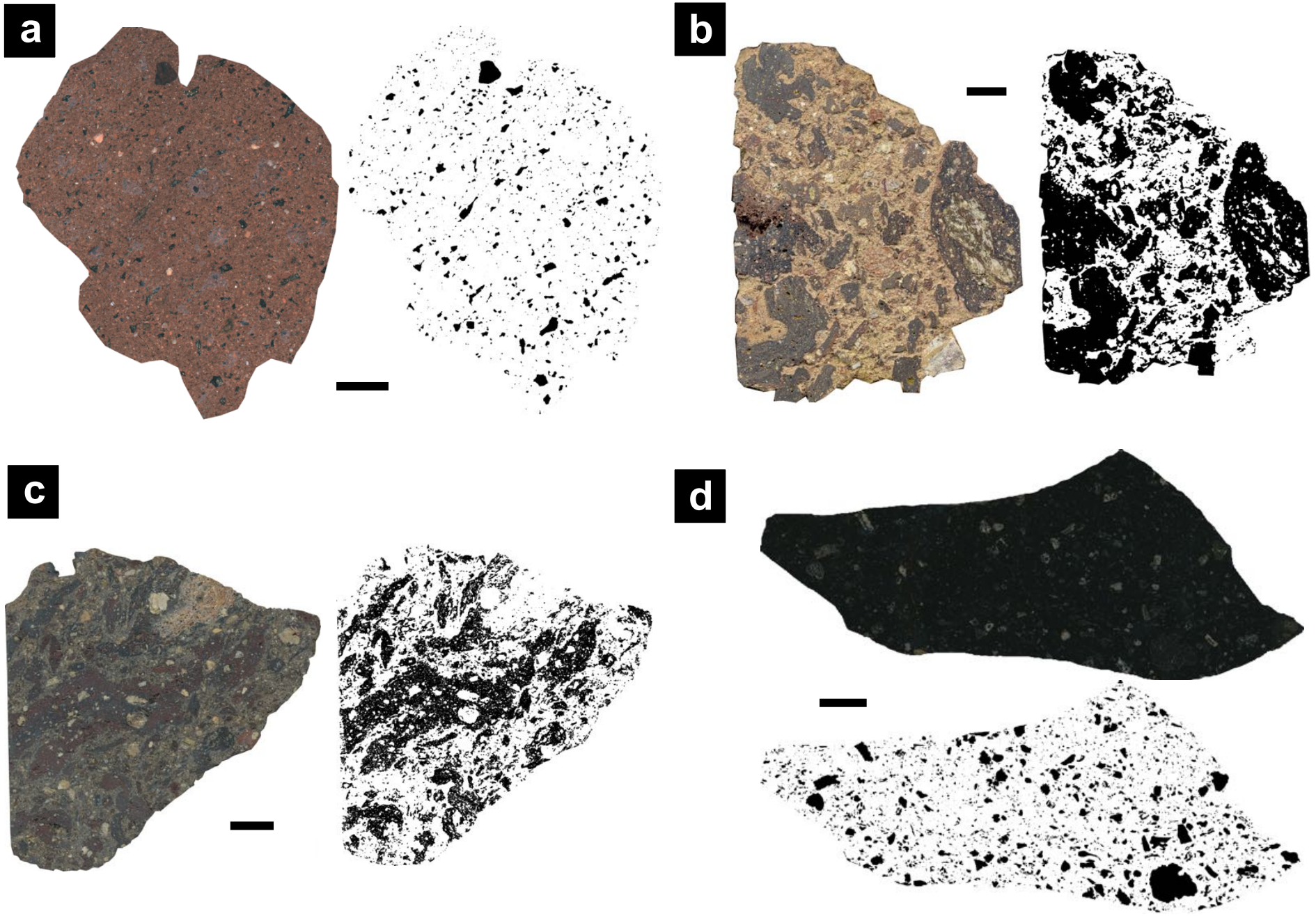
a
b
c
d

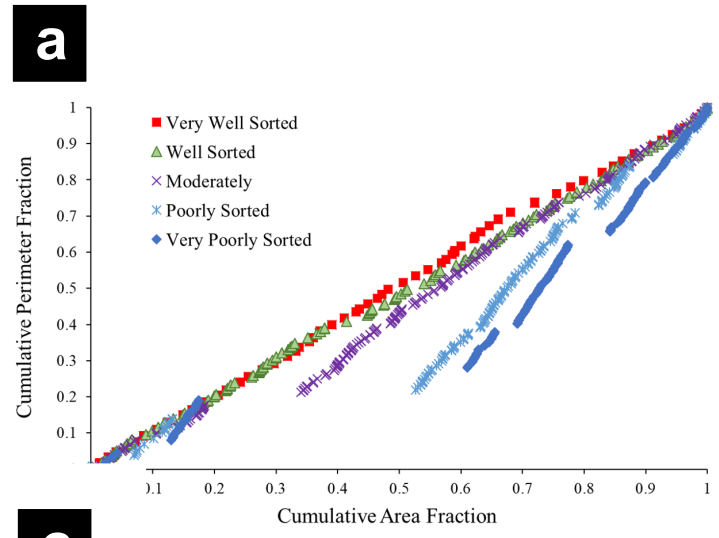
a
Very Well Sorted
Well Sorted
Moderately
Poorly Sorted
Very Poorly Sorted
Cumulative Perimeter Fraction
Cumulative Area Fraction

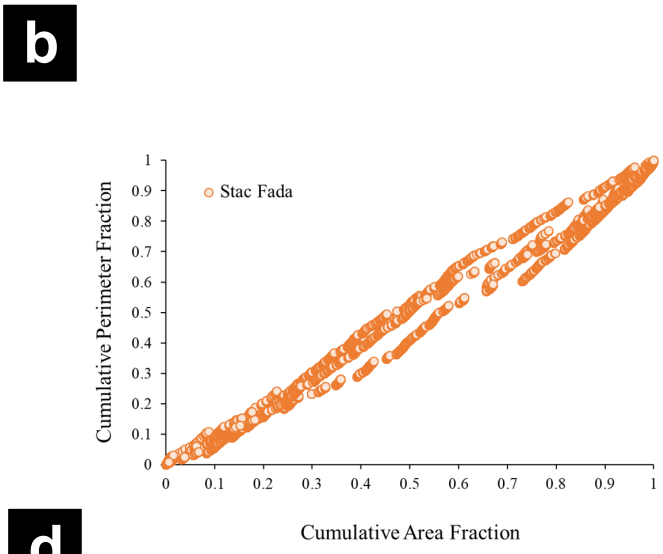
b
Stac Fada
Cumulative Perimeter Fraction
Cumulative Area Fraction

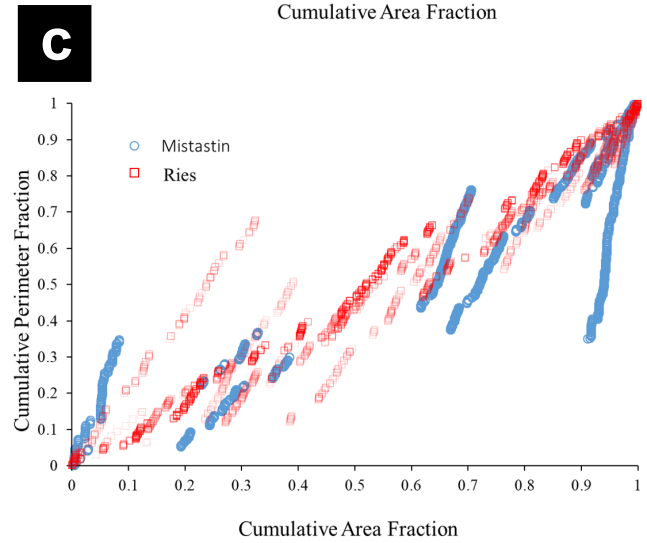
c
Mistastin
Ries
Cumulative Perimeter Fraction
Cumulative Area Fraction

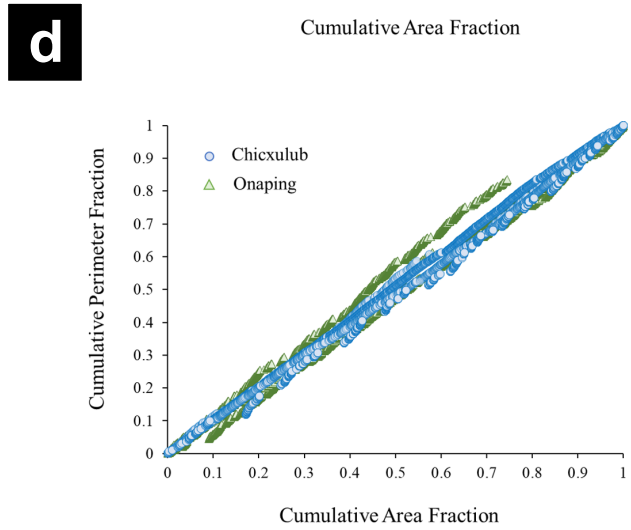
d
Chicxulub
Onaping
Cumulative Perimeter Fraction
Cumulative Area Fraction

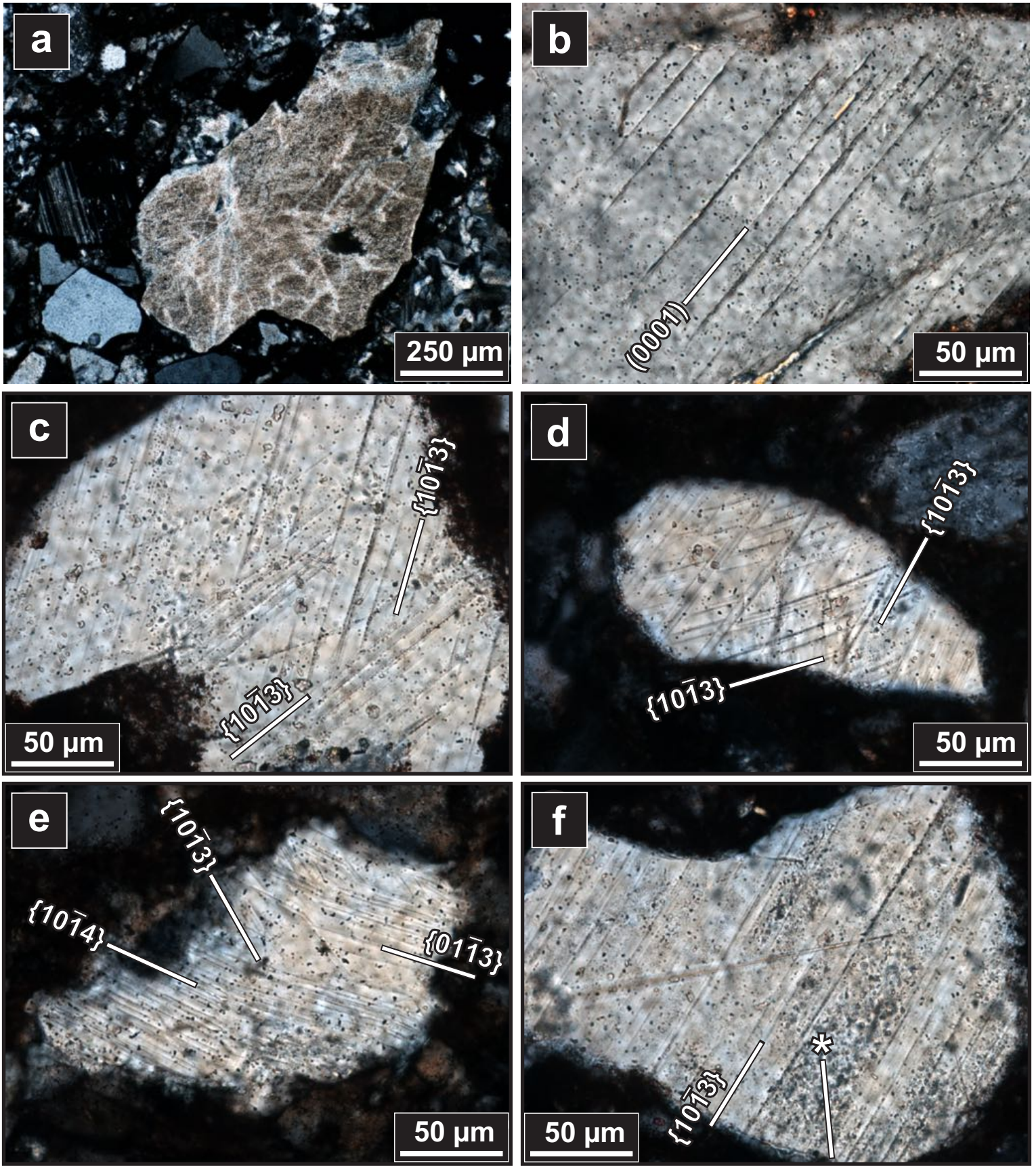
a
250 µm
b
(0001)
50 µm
c
{10$\bar{1}$3}
{10$\bar{1}$3}
50 µm
d
{10$\bar{1}$3}
{10$\bar{1}$3}
50 µm
e
{10$\bar{1}$3}
{10$\bar{1}$4}
{01$\bar{1}$3}
50 µm
f
{10$\bar{1}$3}
*
50 µm

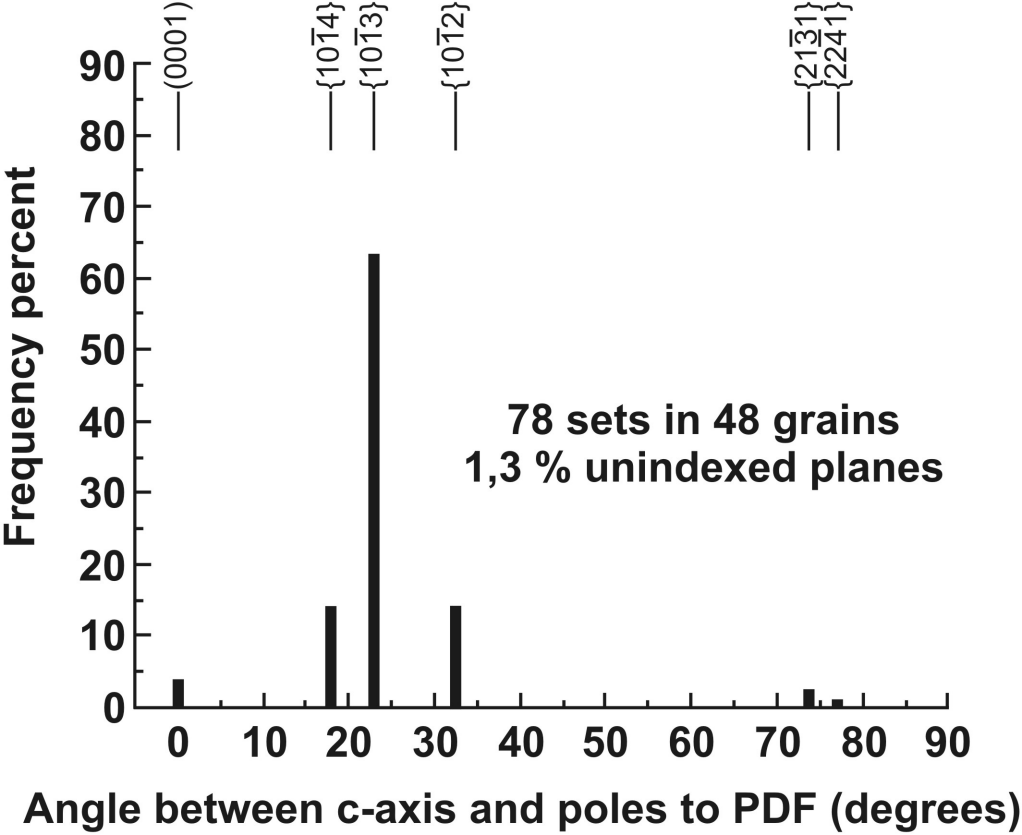
(0001)
{10$\bar{1}$4}
{10$\bar{1}$3}
{10$\bar{1}$2}
{21$\bar{3}$1}
{2241}
78 sets in 48 grains
1,3 % unindexed planes
Frequency percent
0
10
20
30
40
50
60
70
80
90
Angle between c-axis and poles to PDF (degrees)